International Journal of Mass Spectrometry 303 (2011) 31–41

Contents lists available at ScienceDirect

International Journal of Mass Spectrometry

journal homepage: www.elsevier.com/locate/ijms

Escape of high mass ions due to initial thermal energy and its implications for axially symmetric RF ion trap mass analyzer design

E.K. Ganapathy Subramanyan [a], Atanu K. Mohanty [a,b,*]

[a] Department of Instrumentation and Applied Physics, Indian Institute of Science, Bangalore 560012, India
[b] Supercomputer Education and Research Centre, Indian Institute of Science, Bangalore 560012, India

ARTICLE INFO

Article history:
Received 11 August 2010
Received in revised form
17 December 2010
Accepted 19 December 2010
Available online 5 January 2011

Keywords:
Mechanism of ion loss
Sensitivity
Thermal energy
Escape velocity
RF trap design
Nonlinear ion trap mass analyzer.

ABSTRACT

This paper investigates the loss of high mass ions due to their initial thermal energy in ion trap mass analyzers. It provides an analytical expression for estimating the percentage loss of ions of a given mass at a particular temperature, in a trap operating under a predetermined set of conditions. The expression we developed can be used to study the loss of ions due to its initial thermal energy in traps which have nonlinear fields as well as those which have linear fields.

The expression for the percentage of ions lost is shown to be a function of the temperature of the ensemble of ions, ion mass and ion escape velocity. An analytical expression for the escape velocity has also been derived in terms of the trapping field, drive frequency and ion mass.

Because the trapping field is determined by trap design parameters and operating conditions, it has been possible to study the influence of these parameters on ion loss. The parameters investigated include ion temperature, magnitude of the initial potential applied to the ring electrode (which determines the low mass cut-off), trap size, dimensions of apertures in the endcap electrodes and RF drive frequency.

Our studies demonstrate that ion loss due to initial thermal energy increases with increase in mass and that, in the traps investigated, ion escape occurs in the radial direction. Reduction in the loss of high mass ions is favoured by lower ion temperatures, increasing low mass cut-off, increasing trap size, and higher RF drive frequencies. However, dimensions of the apertures in the endcap electrodes do not influence ion loss in the range of aperture sizes considered.

1. Introduction

This paper revisits and extends the discussion on an old question in the mass spectrometry literature related to ion loss processes in ion trap mass spectrometers. It investigates the ion loss due to initial thermal energy associated with ions. An analytical expression to compute the percentage of ions lost, for a given trap with a set of operating conditions for ions at a given temperature and given mass, has been derived. The theory we developed in this work is applicable to both the axially symmetric three-dimensional [1,2] and two-dimensional [3,4] configurations of ion traps, although analytical expressions for ion loss have been derived only for axially symmetric three-dimensional geometries.

Ion loss, which limits the sensitivity of a mass spectrometer, is known to occur on account of several factors. Space charge effects and scattering due to gas phase reactions such as ion–ion and ion–neutral molecule interactions [5] have been discussed as important mechanisms for ion loss. The extent of ion loss in these processes is a function of the density of ions within the trap at a given pressure [6]. Other ion loss processes that have been discussed in the literature include nonlinear resonances [7,8] and unstable trajectories [5], which include trajectories that are mathematically or quasi unstable. An issue which has received only marginal attention in the mass spectrometry literature [5,9,10] is the loss of ions due to its initial thermal energy.

In ideal traps which have linear fields, an expression for loss of ions due to its high thermal energy can be derived from the linear averaged equation of motion [11]. This model enables the computation of the well depth. All ions having energies larger than the well depth will escape from the trap. However, when the field within the trap is not linear, as in the case of the experimental trap [12] and in traps with newer geometries [2,13,14,4], the expressions derived using the linear averaged equation can, at best, provide only a qualitative insight. For traps that have nonlinear trapping fields, there is a need to develop an expression for ion loss which has compa-

* Corresponding author at: Supercomputer Education and Research Centre, Indian Institute of Science, Bangalore 560012, India. Tel.: +91 80 2293 2487; fax: +91 80 2360 0135.
E-mail addresses: ganasubbu@isu.iisc.ernet.in (E.K. Ganapathy Subramanyan), amohanty@serc.iisc.ernet.in (A.K. Mohanty).

1387-3806/$ – see front matter © 2010 Elsevier B.V. All rights reserved.
doi:10.1016/j.ijms.2010.12.013

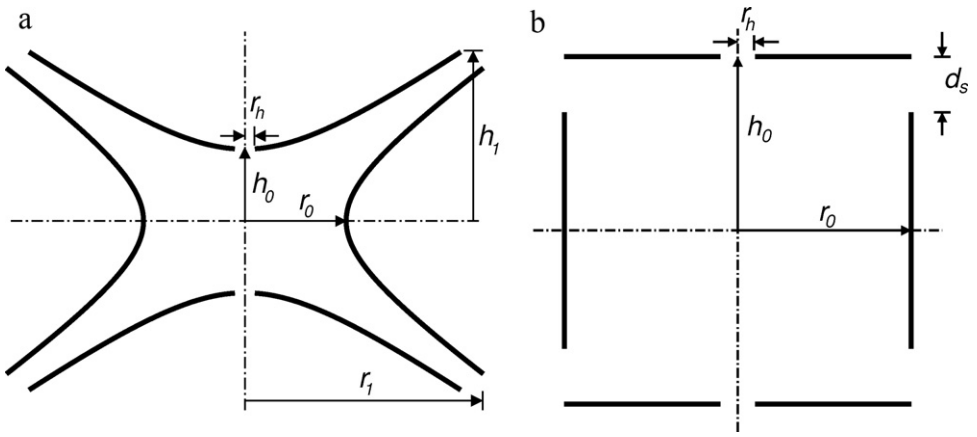

Fig. 1. Cross-sectional views and geometry parameters of (a) QIT and (b) CIT0. CITopt differs from the CIT0 only in its dimensions.

rable accuracy to the expression derivable for linear traps. Such an expression will enable designers to model achievable sensitivities in their traps.

The method we adopted to obtain an analytical expression for the loss of high thermal energy ions is the following: it is known that an ensemble of ions of a given mass has a velocity distribution which, for ion densities below the space charge limit, is determined by its temperature. For a given mass, the higher the temperature, higher will be the ion's root-mean-square velocity and the broader its velocity distribution curve. In our study we have used the Maxwell velocity distribution [15] to describe the velocity distribution of the ensemble. On the other hand, ions of a given mass have an escape velocity, v_{esc}, which is a function of the trapping field they experience. Escape velocity of an ion is defined as the minimum velocity required by an ion situated at the centre of the trap[1], to escape from the trap [16–18]. Escape velocity is not dependent on the temperature of the ion. By mapping v_{esc} for an ion of given mass onto its velocity distribution curve at the specified temperature, it is possible to compute the percentage of ions which have velocities larger than v_{esc}. This percentage corresponds to the ions lost from the trap on account of its initial thermal energy.

As a caveat we point out that because we choose a Maxwell velocity distribution for ions, our study pertains to only those ions that are located at the centre of the trap where the field is zero. Our study therefore ignores other energetic ions throughout the volume of the trap such as those ions which have picked up high energy due to RF heating [19,20], high energy ions formed by dissociation [21] or the ones with high kinetic energy injected into the trap from an external source [22]. In this sense, the results we present are underestimates of the actual number of high energy ions lost from the trap.

In contrast to our approach, researchers who study evaporative cooling of ions [23–26] developed a rate constant based expression for ion loss for specific ion species. In those studies, because the expressions are obtained by fitting experimental data, the expression takes into account thermalization of the ion population and also includes loss of all high energy ions, in addition to those located at the centre of the trap. Our simulation, however, is not concerned with the specific ion species, instead it uses only the mass of the fragment ion. Further, we ignored thermalization and have instead computed ion loss using the velocity distribution corresponding to the initial temperature of the ions. The reason for ignoring thermalization of the ion population and ions away from the trap centre is on account of the difficulty in modelling them.

The expression we present is a function of field within the trap and the escape velocity of the ion. On account of this it has been possible to evaluate the consequences of changing trap parameters on the loss of ions due to its thermal energy. The parameters we discuss in the present paper include ion temperature, low mass cut-off (LMCO), trap size, dimension of the aperture in the endcap electrodes and RF drive frequency.

In Section 2, geometries used in this paper are discussed. Numerical techniques used for calculating field distributions and verification of analytical expressions are outlined in Section 3. Section 4 presents the ion loss calculations and an expression for estimating the escape velocity of the ions has been derived. In the penultimate section of this paper, Section 5, we present plots for the verification of the analytical expression for escape velocity, after which we describe the ion loss curves obtained to understand the effect of different operating parameters. Section 6 presents a few concluding remarks.

2. Geometries considered

Three geometries have been considered in this paper. These include two well studied geometries viz., the quadrupole ion trap, QIT [1] with hyperboloid shaped electrodes and the cylindrical ion trap, CIT0 [2], and an arbitrary geometry, CITopt [27].

Fig. 1 presents the cross-sectional views and geometry parameters of the QIT and the CIT0. CITopt has the same cross-sectional view as the CIT0 but has different dimensions. In the figure, the parameter labelled r_0 refers to the radius of the ring electrode and h_0 to the half-distance between the two endcap electrodes. Other parameters correspond to the dimensions of the apertures in the endcap electrodes (r_h), and the inter-electrode spacing (d_s). Trap dimensions, in mm, used in our simulations are given in Table 1. For the QIT, the parameters h_1 and r_1 indicate the truncation used along the axial and radial directions, respectively.

In our simulations, the endcaps are grounded and the ring electrode is excited with a potential given by

$$\Phi = U + V \sin(\Omega t + \psi_0). \quad (1)$$

Table 1
Geometry parameters of the QIT, CIT0 and CITopt. All dimensions are in mm.

Geometry	h_0	r_0	r_h	d_s	h_1	r_1
QIT	3.5355	5	0.5	–	8.3169	11.762
CIT0	5	5	0.5	1.6	–	–
CITopt	7.7743	5	0.5	1.6	–	–

[1] Trap centre refers to the zero field position in the trap. For traps with top-bottom symmetry, this position is the same as the geometric centre. In asymmetric traps, which do not have top-bottom symmetry, the zero field position is different from its geometric centre.

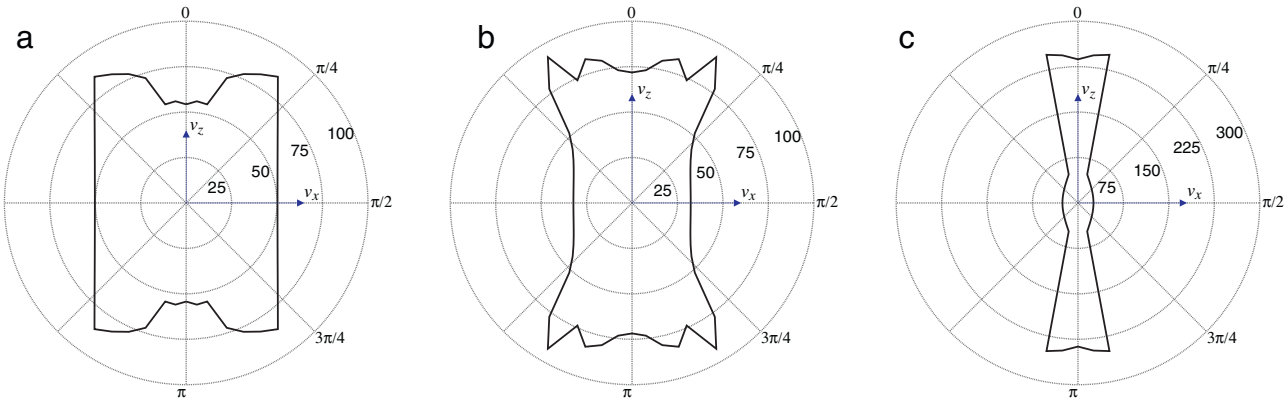

Fig. 2. Variation of escape velocity as a function of velocity angle in the (a) QIT, (b) CIT0 and (c) CITopt. The radial distance in this polar plot indicates velocity in m/s. θ values are indicated on the periphery only on the right half. Angles on the left half are omitted as they are same as those on the right half.

Here U is the DC potential, V is the zero-to-peak amplitude of the RF potential, Ω is the angular frequency and ψ_0 is the phase angle. In all our simulations U is kept at 0 V.

3. Computational methods

This section describes the numerical methods used for the verification of our analytical expressions as well as for computing fields and multipole expansion coefficient, A_2 [28].

3.1. Field and multipole computation

The boundary element method (BEM) reported in Tallapragada et al. [27] has been used to define geometries and specify potential on the electrode to estimate charge distribution on the electrodes. This charge distribution in turn is used to evaluate the fields and the multipole expansion coefficients.

The quadrupole expansion coefficient A_2 is used to compute the modified Mathieu parameter [29,30], $\hat{q}$, defined by the expression:

$$\hat{q} = \frac{4eVA_2}{mr_0^2\Omega^2}, \tag{2}$$

where V is the zero-to-peak RF potential applied across the electrode in volts, Ω is the angular frequency of the RF drive in radians per second, and r_0 is the normalizing length in meters which in our case is the radius of the ring electrode. $\hat{q}$ is the Mathieu parameter for the linearized equation of motion in ion traps with nonlinear fields and is used to distinguish it from the Mathieu parameter q which is associated with the canonical form of the Mathieu equation [31,1].

3.2. Trajectory and escape velocity computation

The trajectory calculations are carried out using the Runge-Kutta fourth order integration routine with the forces acting on an ion (due to the field), the initial velocity (adjusted iteratively till ion escape) and the initial position (set to trap centre) of the ion as inputs. The trajectory is allowed to evolve over a prespecified large time.

This prespecified time allowed for the trajectories to evolve varies with the $\hat{q}$ value of the mass. This is because the secular frequency of the ion varies with its $\hat{q}$, with higher masses having lower $\hat{q}$ and lower secular frequencies. Consequently larger number of RF cycles are required to cover one period of secular oscillation as $\hat{q}$ decreases. This results in larger integration times being required for ions having lower $\hat{q}$. During these computations, ion oscillation amplitude is compared with dimension of the trap boundary and a flag is set whenever the ion oscillation amplitude exceeded the boundary of the trap. The initial velocity for which the ion amplitude became equal to the dimensions of the trap is recorded as the escape velocity of the ion of the chosen mass.

For computing the escape velocity of the ion numerically, we adopt the method outlined in Krishnaveni et al. [18]. Fig. 2 shows polar plots for escape velocity in the v_x–v_z plane, for the QIT, the CIT0 and the CITopt obtained for RF phase angles varying from 0 to 2π in steps of $\pi/6$ and velocity angles varying from 0 to $\pi/2$ in steps of $\pi/30$. To generate these plots, the ion mass is fixed at 1000 Th, the RF drive frequency is kept at 1 MHz and the potentials applied to the ring electrodes are 23.248 V, 31.426 V and 97.463 V for the QIT, CIT0 and CITopt, respectively. The escape velocities are computed only in the first quadrant, the curves in the other quadrants are generated using the symmetry of the trap. It may be seen from the figure that in these three traps, the escape velocity in the radial direction is lower than in any other direction. In view of this, the radial direction is chosen for deriving an expression for escape velocity.

Further, following the observation of Krishnaveni et al. [18] that escape velocity minima occurred at specific combination of RF phase angle and velocity angle, we investigated if such angles exists for axially symmetric traps too. During the simulations carried out for generating the polar plots, it is observed that the escape velocity in any direction occurred at only two RF phase angles, $\pi/2$ and $3\pi/2$. It is further observed that in the radial direction (which is the direction of ion escape with minimum velocity in these traps as pointed out above) the minimum always occurred at RF phase angle of $\pi/2$. Based on these observations, to save computation time, in this paper we limited our calculations to four phase angles corresponding to 0, $\pi/2$, π and $3\pi/2$ and fixed the velocity angle to $\pi/2$. From this set of 4 values for velocities, the minimum is chosen as the escape velocity of the ion in the radial direction.

4. Analytical expression for estimating percentage ion loss versus mass

In the present study the Maxwell velocity distribution function is used to describe the velocity distribution of an ensemble of ions associated with a mass m at a given temperature T. The corresponding probability density function is given by [15]:

$$p(v_x, v_y, v_z) = \left(\frac{m}{2\pi kT}\right)^{3/2} \exp\left(-\frac{mv^2}{2kT}\right), \tag{3}$$

where $v^2 = v_x^2 + v_y^2 + v_z^2$, with v_x, v_y and v_z representing velocities in the respective directions.

Table 2
Comparison of ion loss estimated using Eq. (11) with that calculated using Eq. (8), for a mass of 1000 Th in the QIT, CIT0 and CITopt.

Trap geometry	Percentage ion loss	
	Eq. (8), $\mathcal{L}$	Eq. (11), $\mathcal{L}_{cyl}$
QIT	66.547	59.7509
CIT0	78.4160	80.9727
CITopt	90.944	87.5551

The ion loss, $\mathcal{L}$, can be formulated by writing Eq. (3) in the spherical coordinate system as

$$\mathcal{L} = \left(\frac{m}{2\pi kT}\right)^{3/2} \int_0^{2\pi} \int_0^{\pi} \int_{v_{th}(\theta)}^{\infty} v^2 \exp\left(-\frac{mv^2}{2kT}\right) \mathrm{d}v \sin\theta \,\mathrm{d}\theta \,\mathrm{d}\phi, \tag{4}$$

where $v_{th}(\theta)$ is the escape velocity of the ion when the ion is launched at an angle θ with respect to the axial direction.

Since there is no dependence on ϕ, the above integral can be written as

$$\mathcal{L} = \left(\frac{m}{2kT}\right)^{3/2} \frac{2}{\sqrt{\pi}} \int_0^{\pi} \int_{v_{th}(\theta)}^{\infty} v^2 \exp\left(-\frac{mv^2}{2kT}\right) \mathrm{d}v \sin\theta \,\mathrm{d}\theta. \tag{5}$$

Due to the symmetry of the trap we have $v_{th}(\theta) = v_{th}(\pi - \theta)$, this further reduces our integral to

$$\mathcal{L} = \left(\frac{m}{2kT}\right)^{3/2} \frac{4}{\sqrt{\pi}} \int_0^{\pi/2} \int_{v_{th}(\theta)}^{\infty} v^2 \exp\left(-\frac{mv^2}{2kT}\right) \mathrm{d}v \sin\theta \,\mathrm{d}\theta. \tag{6}$$

The substitution $u = (v/\sqrt{(2kT/m)})$ into Eq. (6) yields

$$\mathcal{L} = \frac{4}{\sqrt{\pi}} \int_0^{\pi/2} \int_{\frac{v_{th}(\theta)}{\sqrt{(2kT/m)}}}^{\infty} u^2 \exp(-u^2) \,\mathrm{d}u \sin\theta \,\mathrm{d}\theta. \tag{7}$$

Integrating by parts the inner integral of Eq. (7) over the given limits, the final expression for computing ion loss is

$$\mathcal{L} = \int_0^{\frac{\pi}{2}} \left[\frac{2v_{th}(\theta)}{\sqrt{(2\pi kT/m)}} \exp\left(-\frac{mv_{th}^2(\theta)}{2kT}\right) + \mathrm{erfc}\left(\frac{v_{th}(\theta)}{\sqrt{(2kT/m)}}\right) \right] \sin\theta \,\mathrm{d}\theta. \tag{8}$$

Eq. (8), when integrated, provides the fraction of ions which have velocities greater than v_{th}, along the corresponding initial velocity direction, for a specified mass and temperature. More detailed derivation for the ion loss formulation is given in Ganapathy Subramanyan [32].

While Eq. (8) provides an accurate estimate of ion loss, it does not lend itself to providing an analytical expression for ion loss since the escape velocity surfaces for the different ion traps (as seen in Fig. 2) are irregular and do not have an analytical formulation. In this paper Eq. (8) has been used only when ion loss is estimated numerically for the purpose of verifying the accuracy of the analytical approximation that we derive (see Table 2). To obtain an analytical expression for ion loss we will need to approximate the escape velocity surface with a simpler surface.

A clue to what this approximate, but well characterized, surface may look like can be obtained by an inspection of the escape velocity surfaces in Fig. 2. In these plots it is seen that for the most part, especially for the QIT and CIT0 and to a lesser extent for the CITopt, the cross section of the escape velocity volume can be approximated by two straight lines parallel to the v_z-axis. When this is done the volume within which ions are stable can be approximated

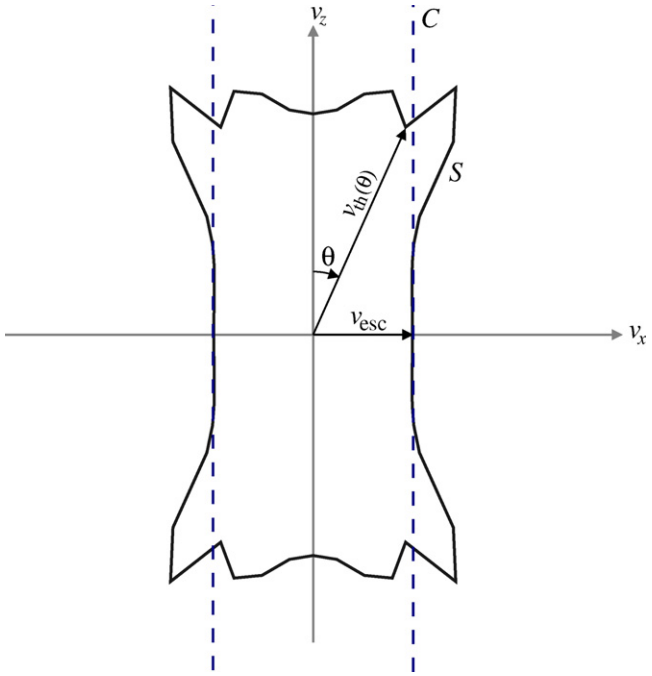

Fig. 3. Escape velocity profile for the CIT0 obtained from Fig. 2(b). Surfaces *S* and *C* have been labelled in the figure.

by a cylinder. Further, from the point of view of ease of computation, in the present paper we have considered the escape velocity surface to be an infinite cylinder rather than a truncated one. The cross section of the infinite cylinder has been shown in Fig. 3 as dashed lines on the escape velocity profile for the CIT0 taken from Fig. 2(b). Its surface is labelled *C*. The radius of the cylinder is taken to be the waist of surface *S*. Also shown in the figure are parameters $v_{th}(\theta)$ and the angle θ which are used in Eq. (8) for computing the percentage of ions lost.

Using the approximation of the infinite cylinder, Eq. (3) is now rewritten in cylindrical coordinates to obtain the fraction of ions lost, $\mathcal{L}_{cyl}$, as

$$\mathcal{L}_{cyl} = \int_{-\infty}^{\infty} \sqrt{\frac{m}{2\pi kT}} \exp\left(-\frac{mv_z^2}{2kT}\right) \mathrm{d}v_z \int_0^{2\pi} \mathrm{d}\phi \int_{v_{esc}}^{\infty} \frac{m}{2\pi kT} \exp\left(-\frac{mv_\rho^2}{2kT}\right) v_\rho \,\mathrm{d}v_\rho, \tag{9}$$

where $v_\rho^2 = v_x^2 + v_y^2$ and $\phi = \arctan(v_y/v_x)$. Here, the first integral term evaluates to 1 and the second evaluates to 2π. Substituting these values into Eq. (9) we get:

$$\mathcal{L}_{cyl} = \int_{v_{esc}}^{\infty} \frac{m}{2kT} v_\rho \exp\left(-\frac{mv_\rho^2}{2kT}\right) \mathrm{d}v_\rho. \tag{10}$$

The above integral is simplified by substituting $u = (mv_\rho^2/\sqrt{2kT})$ in Eq. (10), and it simplifies to the form:

$$\mathcal{L}_{cyl} = \int_{\frac{mv_{esc}^2}{2kT}}^{\infty} e^{-u} \,\mathrm{d}u = \exp\left(-\frac{mv_{esc}^2}{2kT}\right). \tag{11}$$

Eq. (11) is the analytical approximation for evaluating ion loss which we will be using in this paper.

In order to see how well Eq. (11) approximates the results obtained using Eq. (8), we present in Table 2 the percentage loss of ions for the three geometries QIT, CIT0 and CITopt. In the computations to obtain the v_{th} values, the ion mass is fixed at 1000 Th, the RF drive frequency is set to 1 MHz and the endcaps are kept at ground potential. To set the LMCO as 10 Th, the potentials applied

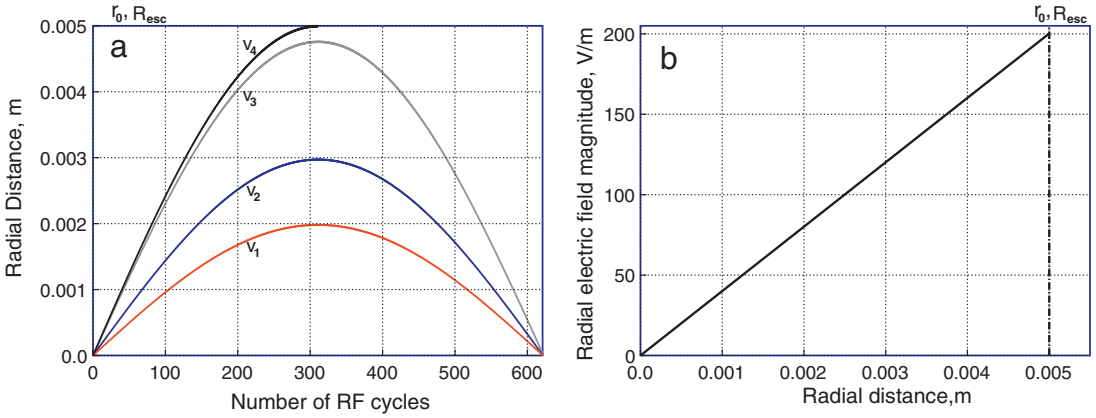

Fig. 4. (a) Ion trajectories in QIT for different initial velocities; v_1=10 m/s, v_2=15 m/s, v_3=24 m/s and v_4= 25.191 m/s. (b) Magnitude of electric field along radial direction for the QIT.

to the ring electrodes are 23.248 V, 31.426 V and 97.463 V for the QIT, CIT0 and CITopt, respectively. In all cases, Eq. (8) is integrated using the Simpson's rule [33] and the ion losses are calculated for an ion temperature of 298.15 K.

From the table, it is seen that the approximation predicts the fraction of ions lost closely to that given by Eq. (8) for all traps. Except in case of the CIT0, the ion loss estimated by Eq. (11) gives a lower bound for the percentage of ions lost. In case of the CIT0, it is seen from the polar plot presented in Fig. 2(b) that, a region in the polar plot lies outside the cylinder with radius v_{esc}. Due to this, ions whose escape velocities lie outside the cylinder of approximation, though within the region inside polar plot are counted as lost. In such cases the loss estimated by the expression provided in Eq. (11) is slightly higher than that calculated through Eq. (8).

4.1. Escape velocity, v_{esc}

In this section an analytical expression for computing the escape velocity, v_{esc}, for an ion of mass m, in a specified trap geometry for a set of operating conditions, is developed. When this expression for v_{esc} is inserted into Eq. (11), it will provide the necessary expression for obtaining the fraction of ions lost for a particular mass, at a given temperature.

Before deriving an expression for v_{esc}, we briefly digress to discuss two parameters, R_{esc} and $E_{r,peak}(R_{esc})$, which will appear in the expression for v_{esc}. This will be done by (1) tracing ion trajectories for different initial velocities and (2) plotting radial fields in the ion traps.

In this study we consider two traps, the QIT and the CIT0, the QIT having no apertures in the endcap electrodes and the CIT0 with an aperture dimension of 0.5 mm (corresponding to 10% of the ring electrode radius) as shown in Table 1. The other geometry parameters remain the same as mentioned in that table.

For the ion trajectory studies mass is set to 2000 Th, drive frequency is fixed at 1 MHz and the endcaps are kept at ground potential. The potentials applied to the ring electrodes are 23.248 V and 31.426 V for QIT and CIT0, respectively, so as to set LMCO to 10 Th in the two traps. For the QIT, the trajectories are traced for initial ion velocities of 10.0 m/s, 15.0 m/s, 24.0 m/s and 25.191 m/s. For the CIT0 the trajectories are traced for initial ion velocities of 10.0 m/s, 14.5 m/s, 16.16 m/s and 16.1678 m/s. In all these simulations, the initial position is set as the trap centre. The results of these simulations are presented in Figs. 4(a) and 5(a) for the QIT and CIT0, respectively.

For the field studies, the electric field is computed in the two traps for an applied unit potential to the ring electrodes with the endcaps grounded. The magnitude of electric fields along the radial direction inside the QIT and CIT0 are shown in Figs. 4(b) and 5(b), respectively.

We first investigate the trajectory plots (Fig. 4(a)) obtained for the QIT. For the QIT, the amplitude of secular oscillations gradually increases as the initial ion velocity is increased. When the initial velocity reaches 25.191 m/s the ion oscillation amplitude equals the trap dimension and ion escape occurs. The distance from the centre of the trap to the point at which ion escape occurs is designated as R_{esc}. As seen in this plot for the QIT, since ion escape occurs at the ring electrode boundary, R_{esc} equals the radius of the ring electrode.

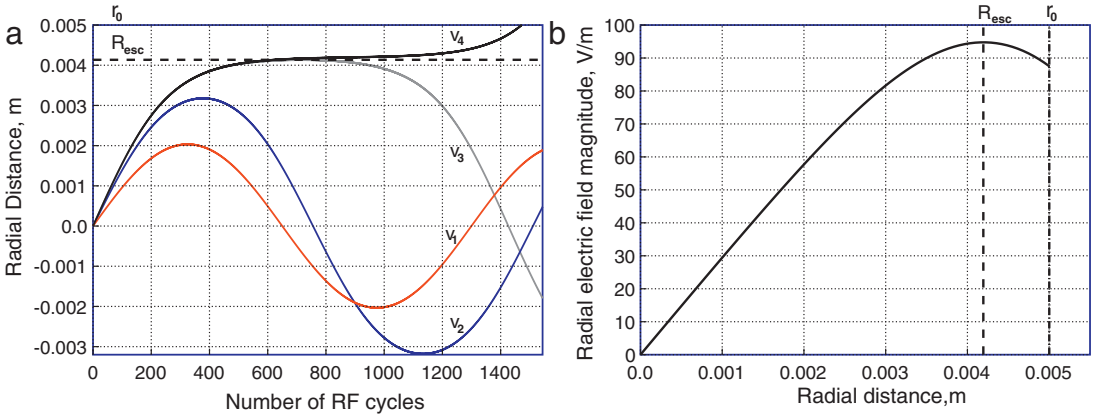

Fig. 5. (a) Ion trajectories in CIT0 for different initial velocities; v_1=10 m/s, v_2=14.5 m/s, v_3=16.16 m/s and v_4= 16.1678 m/s. (b) Magnitude of electric field along radial direction for the CIT0.

Further, as can be surmised from Fig. 4(a), at R_{esc} the ion velocity is zero and, as can be seen in Fig. 4(b), at R_{esc} the field is maximum. This maximum field is defined as $E_{r,peak}(R_{esc})$. For the QIT under study, R_{esc} is 0.005 m and $E_{r,peak}(R_{esc})$ is 200.090 V/m.

Turning to the CIT0 and Fig. 5(a), here too we see that the amplitude of ion oscillation increases as the initial ion velocity is increased. There is, however, a different mechanism for ion escape as can be seen for the plot corresponding to the initial ion velocity of 16.1678 m/s. Unlike the case of the QIT, for the CIT0, after the ion trajectory plateaus off, the trajectory dramatically changes direction and the ion gets destabilized. In such traps it is this distance from the centre of the trap, where ion destabilization occurs, which is used to define R_{esc}. Here too the velocity of ion motion is zero at R_{esc}. Also, at R_{esc} the field plot (Fig. 5(b)) reveals that the field is maximum. In such traps it is this field maximum that is used to define $E_{r,peak}(R_{esc})$. For the CIT0 under discussion, R_{esc} is 0.0042 m and $E_{r,peak}(R_{esc})$ is 94.760 V/m.

We remind that $E_{r,peak}(R_{esc})$, which refers to the maximum field in the radial direction is actually the minimum field amongst the field maxima that are computed in all directions. It is on account of this that ion escape occurs in the radial direction with least escape velocity. An intuition about this can be obtained by inspecting the escape velocity polar plots shown in Fig. 2 where it can be seen that the escape velocity is minimum in the radial direction.

As an interesting aside, we draw attention to the trajectory plots (Fig. 4(a) and 5(a)). For the QIT, which has a predominantly linear field, the zero-crossings of all the trajectories are very close to each other indicating that the secular frequency changes only slightly with the oscillation amplitude. On the other hand, for the CIT0, in which the field is more nonlinear compared to the QIT, there is a noticeable change in secular frequency with amplitude, as indicated by the wide separation in the zero-crossings of the trajectories. The secular frequency decreases with increasing oscillation amplitude.

We now return to derive an analytical expression for the escape velocity.

In order to derive an analytical expression for v_{esc}, an averaged equation of motion for an ion of mass m within a trap with a specified field and specified set of operating conditions is first developed. From this averaged equation of motion, we derive an expression for v_{esc}, which, when substituted into the equation for the percentage of ion loss, provides us the expression we seek. We begin by defining the field inside the trap at any point along the radial direction as

$$E_r(r) = E_{r,peak}(r)\cos(\Omega t), \tag{12}$$

where $E_{r,peak}(r)$ is the peak value of the electric field expressed as a function of r inside the ion trap, and Ω is the angular frequency of the RF drive in radians per second. $E_{r,peak}(r)$ for the QIT, for example, has the form:

$$E_{r,peak}(r) = \frac{2rV}{r_0^2 + 2z_0^2} \tag{13}$$

where V is the zero-to-peak RF potential applied across the electrodes. An expression based on multipole expansion coefficients can also be formulated for other axially symmetric traps. In the present study we will not be deriving expressions such as in Eq. (13). Instead, $E_{r,peak}(r)$ will be evaluated numerically.

Using Eq. (12), an equation of motion of the ion within the trap following the method outlined in Major and Dehmelt [19] is derived.

Balancing the forces acting on an ion of mass m and charge e moving in the radial direction, we have

$$m\frac{d^2r}{dt^2} = eE_{r,peak}(r)\cos(\Omega t). \tag{14}$$

Following Wuerker et al. [11], Major and Dehmelt [19], the radial motion of an ion is written as the sum of two components, a displacement ξ, due to the micromotion resulting from the high frequency field, superimposed on the much larger amplitude fundamental secular motion, R, so that $r = R + \xi$. Using the averaging approach similar to that of Major and Dehmelt [19], we obtain the equation of the secular motion as

$$\ddot{R} + \frac{1}{2}\left(\frac{e}{m\Omega}\right)^2 E_{r,peak}(R)E'_{r,peak}(R) = 0. \tag{15}$$

This can be equivalently rewritten as $\frac{d}{dt}[\dot{R}^2 + (1/2)((eE_{r,peak}(R)/m\Omega))^2] = 0$, or,

$$\dot{R}^2 + \frac{1}{2}\left(\frac{eE_{r,peak}(R)}{m\Omega}\right)^2 = (\text{constant}). \tag{16}$$

The constant can be evaluated by recalling the discussion at the start of this section: at $R = R_{esc}$, the ion velocity, $\dot{R}$, is zero. Applying these conditions, the constant of Eq. (16) can be calculated to be

$$\frac{1}{2}\left(\frac{eE_{r,peak}(R_{esc})}{m\Omega}\right)^2,$$

where $E_{r,peak}(R_{esc})$ corresponds to the maximum field in the radial direction. Substituting this value for the constant in Eq. (16), we obtain:

$$\dot{R}^2 + \frac{1}{2}\left(\frac{eE_{r,peak}(R)}{m\Omega}\right)^2 = \frac{1}{2}\left(\frac{eE_{r,peak}(R_{esc})}{m\Omega}\right)^2. \tag{17}$$

To obtain the escape velocity of the ion, we apply the initial conditions which correspond to the state of the ion when it is in the vicinity of the centre of the trap *i.e.*, $\dot{R} = v_{esc}$ and $E_{r,peak}(R) = 0$. Substituting these in Eq. (17), we get the expression for escape velocity as

$$v_{esc} = \frac{eE_{r,peak}(R_{esc})}{\sqrt{2}m\Omega}, \tag{18}$$

$E_{r,peak}(R_{esc})$ is evaluated numerically in all the simulations in this paper. Substituting this expression for v_{esc} in Eq. (11) we obtain:

$$\mathcal{L}_{cyl} = \exp\left(-\frac{(eE_{r,peak}(R_{esc}))^2}{4\Omega^2 mkT}\right). \tag{19}$$

An inspection of Eq. (19) indicates that $\mathcal{L}_{cyl}$ is of the form $\exp(-(\text{constant})/m)$, where m is the mass of the ion, and the constant depends on the trap geometry and operating conditions.

5. Results and discussions

Results of our study on the loss of high mass ions caused by temperature and other operating parameters of the ion trap are presented. These studies use Eq. (11) and are carried out on the CIT0.

Since accuracy of the analytical expression for determining percentage of ion loss (Eq. (11)) is dependent on the accuracy of estimating escape velocity, we begin by validating Eq. (18), which is used to compute v_{esc}. Before we proceed with our study to verify Eq. (18), there is a point that needs to be clarified with regards to the numerical computation of escape velocity. This is with regard to the time the ions take to get destabilized from the trap.

5.1. Number of RF cycles

In this study we use the CIT0 geometry and calculate the escape velocities for ions of five masses 500 Th, 2000 Th, 5000 Th, 8000 Th and 10000 Th, for an applied ring electrode potential of 31.426 V

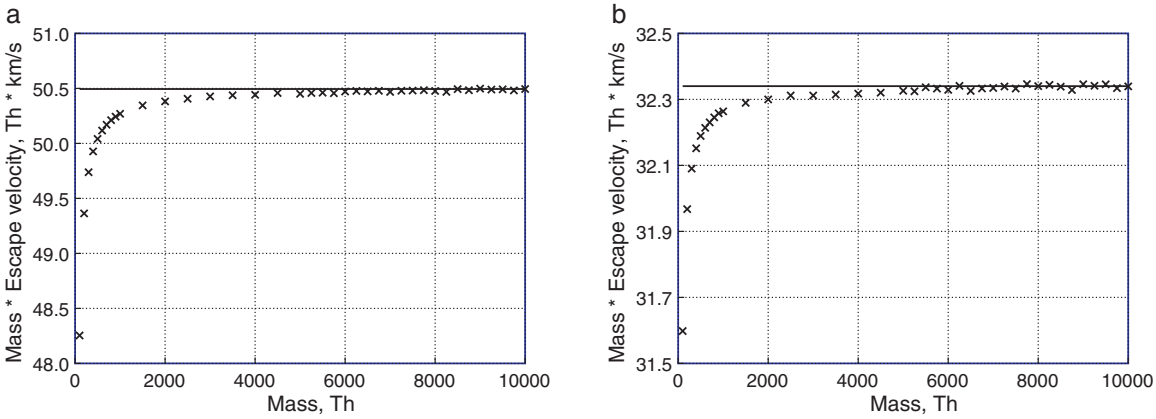

Fig. 6. Plot of ion escape velocity times ion mass versus mass of ion with escape velocity calculated from Eq. (18) (continuous line) and numerical computation (×) for the (a) QIT and (b) CIT0.

Table 3
Comparison of time required for accurate estimation of escape velocity for ions in CIT0.

Mass (in Th)	Number of RF cycles	Time in ms	Escape velocity in m/s
500	330	0.330	64.6750
2000	1472	1.472	16.1678
5000	3534	3.354	6.4672
8000	5021	5.021	4.0425
10000	6376	6.376	3.2339

Table 4
Number of RF cycles for ion destabilization and percentage ion loss for different initial velocities for mass 2000 Th.

Initial ion velocity in m/s	Time taken to escape in terms of RF cycles	Percentage ion loss
16.1678	1472	64.601
16.20	938	64.536
17.20	490	62.510

(so as to set a LMCO of 10 Th) at 1 MHz RF drive frequency. The values for escape velocity and time required to obtain these values are tabulated in Table 3. It may be seen from the table that the number of RF cycles required to estimate escape velocity in the mass range 500–10,000 Th varies from 330 cycles to 6376 cycles; and the corresponding time for a 1 MHz drive frequency is 0.330 ms and 6.376 ms.

While it is true that associated time for these large number of RF cycles is greater than the cooling time associated with the mass spectrometry experiment (either in the mass selective or resonance ejection experiments), we point out that for marginally larger velocities, the number of RF cycles required to destabilize the ion from the trap drastically reduces. In order to see this, we carried out simulation on an ion of mass 2000 Th confined in the CIT0 with aperture dimension as 10% of the ring electrode radius, for an applied potential of 31.426 V to the ring electrode (with endcaps grounded) at 1 MHz drive frequency. The result of this simulation is shown in Table 4. It can be seen from the table that for estimating the escape velocity of 16.1678 m/s, 1472 RF cycles are required, whereas ion ejection occurs in 938 RF cycles for a marginally higher initial ion velocity of 16.20 m/s and 490 RF cycles suffices when the initial ion velocity is 1 m/s higher at 17.20 m/s. The latter two timings are well within the cooling time used in mass spectrometry experiment.

5.2. Verification of Eq. (18)

Verification of Eq. (18) is carried out on both, the QIT (with no apertures in the endcap electrodes) and CIT0 (with dimension of the aperture in the endcap electrodes being 10% of the ring electrode radius). We assume the RF drive frequency to be 1 MHz in our simulations. To obtain $E_{r,\mathrm{peak}}(R_{\mathrm{esc}})$, peak values of the field obtained from the plots (refer Figs. 4(b) and 5(b)) with actual applied voltages on the ring electrode (which fixes the LMCO at 10 Th in these two traps) are multiplied. These potentials correspond to 23.248 V for the QIT and 31.426 V for the CIT0. $E_{r,\mathrm{peak}}(R_{\mathrm{esc}})$ values are reported in Table 5 along with the geometry parameters used.

When the drive frequency, Ω, and the numerically computed $E_{r,\mathrm{peak}}(R_{\mathrm{esc}})$ are inserted into Eq. (18), we can compute ν_{esc} for each mass for a given trap. Fig. 6(a) and (b) presents the product of ion escape velocity and ion mass versus ion mass for the QIT and the CIT0, respectively. As Eq. (18) shows, $\nu_{\mathrm{esc}}m$ is a constant. This is borne out by the horizontal lines in these two figures. In order to check the agreement of Eq. (18) with the numerically obtained values, we plot with crosses (×), the values computed numerically. It can be seen that even at masses as low as 100 Th, Eq. (18) is within 5% of the numerical obtained values. At higher masses, however, the agreement is much better.

In these traps, A_2 has been numerically computed as −1.0053 and −0.7387 for QIT and CIT0, respectively. Using these values of A_2, it is seen that 100 Th corresponds to a $\hat{q}$ close to 0.1 implying that our expression provides a good estimate of escape velocities for $\hat{q}$ values below 0.1, with Eq. (18) making better estimates as $\hat{q}$ decreases.

5.3. Ion loss curves

The results obtained in our study of the loss of high mass ions due to the initial thermal energies of the ions are now presented.

Table 5
Geometry parameters, applied potential and $E_{r,\mathrm{peak}}(R_{\mathrm{esc}})$ of the QIT and CIT0. All dimensions are in mm.

Geometry	h_0	r_0	r_h	d_s	h_1	r_1	Potential applied on ring electrode in V	$E_{r,\mathrm{peak}}(R_{\mathrm{esc}})$ in V/m
QIT	3.5355	5	0.0	–	8.3169	11.762	23.248	4651.7000
CIT0	5	5	0.5	1.6	–	–	31.426	2977.9277

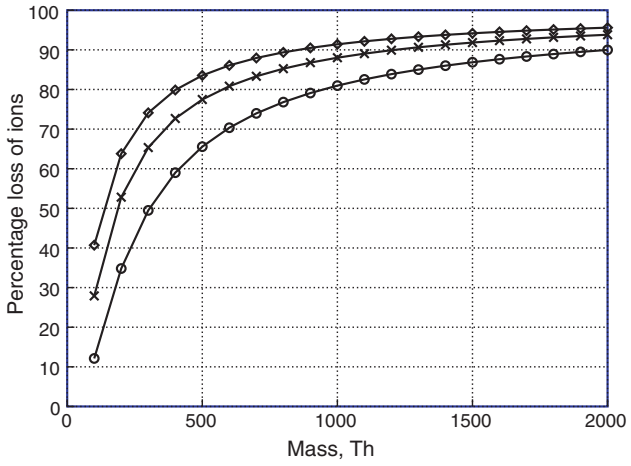

Fig. 7. Percentage loss of ions versus mass for CIT0 at different ion temperatures: 298.15 K (○), 493 K (×) and 700 K (◊).

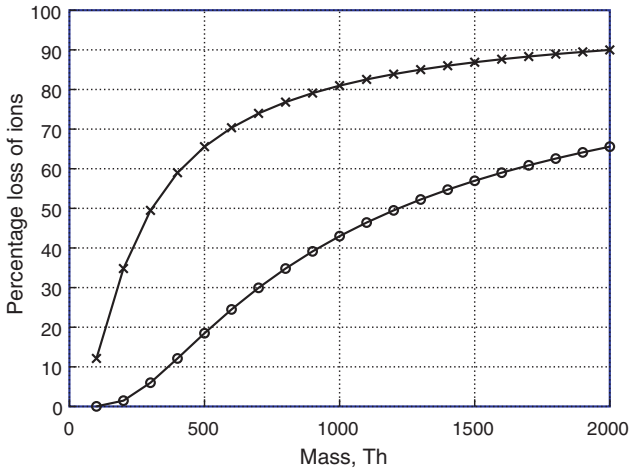

Fig. 8. Comparison of percentage loss of ions versus mass for CIT0 operated at different LMCO: 20 Th (○) and 10 Th (×).

Influence of the following parameters in causing loss of high mass ions are investigated: (1) ion temperature, (2) low mass cut-off, (3) trap size, (4) endcap aperture size, and (5) RF drive frequency. All studies are carried out on the CIT0. To study the effect of temperature, three different ion temperatures, 298.15 K, 493 K and 700 K are considered; to study the effect of LMCO, two different low mass cut-off, 10 Th and 20 Th, are considered; to study the effect of trap size, three different trap sizes, the one as presented in Table 1, a second which is half its size and a third one-tenth its size are considered; to study the effect of endcap aperture size, three different aperture dimensions, 0%, 10% and 30% of the ring electrode radius are considered; to study the effect of RF drive frequency, three different frequencies, 2 MHz, 1 MHz and 500 kHz are considered. The temperature is fixed at 298.15 K for all except ion temperature studies. In all the plots shown, the ion loss evaluated at discrete masses (using Eq. (11)) are joined by a smooth curve.

As will be seen, the ion loss curves have similar variation with mass. This is to be expected because, as pointed out earlier, the ion loss $\mathcal{L}_{cyl}$ in Eq. (19), has the form $\exp(-(\text{constant})/m)$. While it would have sufficed to show just one figure with several curves corresponding to different values of constants, the effect of different parameters on ion loss would not be easily discernible. It is for this reason that we have chosen to display the plots corresponding to each parameter separately.

5.3.1. Ion temperature

The ion loss curves for the CIT0 for three different ion temperatures of 298.15 K, 493 K and 700 K are shown in Fig. 7. For these computations, the RF drive frequency is kept at 1 MHz and the dimension of the aperture in the endcap electrodes is set to 10% of the ring electrode radius of the trap. To set a LMCO of 10 Th, a potential of 31.426 V is applied to the ring electrode (with endcaps grounded) for a computed A_2 value of −0.7387. $E_{r,\text{peak}}(R_{\text{esc}})$ for these sets of parameters are computed to be 2977.9277 V/m.

It is evident from the figure that the lower ion temperature curve displays smaller ion losses compared to the higher ion temperature curves. The 298.15 K curve reveals that ion loss is about 12% for a mass of 100 Th. Thereafter the ion loss increases to about 90% at 2000 Th. The 493 K curve shows that the loss increases from about 28% at a mass of 100 Th to about 93% at a mass of 2000 Th. The 700 K curve indicates that at 100 Th, ion loss is close to 41% and the loss increases to about 95% at a mass of 2000 Th.

5.3.2. Low mass cut-off, LMCO

Fig. 8 shows the ion loss curves for the CIT0 operated for LMCO values of 20 Th and 10 Th. In these computations, the RF drive frequency is kept at 1 MHz, the dimension of the aperture is set to 10% of the ring electrode radius and the ion temperature is fixed at 298.15 K. To set LMCO as 20 Th and 10 Th, the potentials applied to the ring electrodes (with endcaps grounded) are 62.852 V and 31.426 V, respectively. The computed A_2 value is −0.7387. $E_{r,\text{peak}}(R_{\text{esc}})$ for these sets of parameters are computed to be 5955.8555 V/m (for LMCO 20 Th) and 2977.9277 V/m (for LMCO 10 Th). These values are tabulated in Table 6.

Table 6
Numerically computed $E_{r,\text{peak}}(R_{\text{esc}})$ for CIT0 for different LMCO.

LMCO in Th	Potential applied on ring electrode in V	$E_{r,\text{peak}}(R_{\text{esc}})$ in V/m
20	62.852	5955.8555
10	31.426	2977.9277

The curve corresponding to LMCO of 20 Th shows a smaller ion loss compared to the 10 Th curve. It can be seen that the 20 Th curve displays negligible ion loss till a mass of 200 Th after which the ion loss slowly increases to about 66% at 2000 Th. In the case of the 10 Th curve, however, even at 100 Th there is a loss of over 10%.

5.3.3. Trap size

The ion loss curves for three sizes of the CIT0 geometry are presented in Fig. 9. The three sizes considered are the CIT0 whose

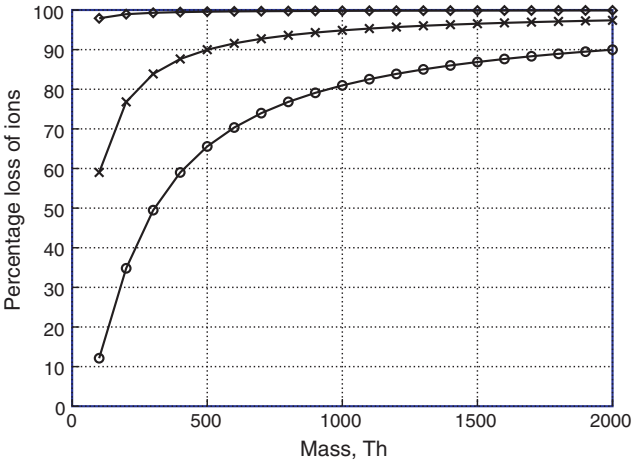

Fig. 9. Comparison of percentage loss of ions versus mass for CIT0 for different scaled geometries: unscaled (○), scaled by half (×) and scaled by one-tenth (◊).

Table 7
Numerically computed $E_{r,peak}(R_{esc})$ for CIT0 for different trap sizes.

Scaling factor	Voltage applied on ring electrode in V	$E_{r,peak}(R_{esc})$ in V/m
No scaling	31.426	2977.9277
Half	7.856	1488.8691
One-tenth	0.314	297.7928

parameters are given in Table 1 and the other two are half and one-tenth the size of the original CIT0. In these computations, the RF drive frequency is fixed at 1 MHz, the endcap aperture is set to 10% of the ring electrode radius, and the ion temperature is set at 298.15 K. To set LMCO to 10 Th, the potentials applied to the ring electrodes (with endcaps grounded) are 31.426 V, 7.856 V and 0.314 V for the original geometry, half-size and one-tenth size CIT0, respectively. The computed A_2 value is −0.7387. $E_{r,peak}(R_{esc})$ for these set of parameters are computed to be 2977.9277 V/m (for the original geometry), 1488.8691 V/m (half-size) and 297.7928 V/m (one-tenth size). These values are tabulated in Table 7.

From the ion loss curves shown, it is evident that there is a lower loss in the case of the full size geometry compared to the scaled down versions of the same geometry. The curve corresponding to the full size geometry shows a loss of about 12% for a mass of 100 Th after which the loss increases to about 90% at 2000 Th. In the case of half-size geometry, lossless trapping is not seen for ions in this mass range and the ion loss increases rapidly to about 90% by 500 Th. In the one-tenth scaled geometry, even at a mass of 100 Th, a loss of about 97% is computed, and the loss rises and reaches close to 99.5% for a mass as low as 500 Th.

5.3.4. Endcap aperture size

Curves in Fig. 10 show the ion loss trends for CIT0 for three different aperture dimensions in the endcap electrode which include 0% (no aperture), 10% and 30% of the trap radius. In these computations, the RF drive frequency is kept at 1 MHz and the ion temperature is set to 298.15 K. To set LMCO to 10 Th, the potentials applied to the ring electrodes (with endcaps grounded) are 31.4 V, 31.426 V and 32.375 V for aperture dimensions 0%, 10% and 30% of trap radius, respectively. $E_{r,peak}(R_{esc})$ for these sets of parameters are computed to be 2976.8142 V/m (for the no aperture case), 2977.9277 V/m (for the 10% aperture) and 3026.3502 V/m (for the 30% aperture). These values are tabulated in Table 8. Numerically computed A_2 values are −0.7397, −0.7387 and −0.7174, respectively.

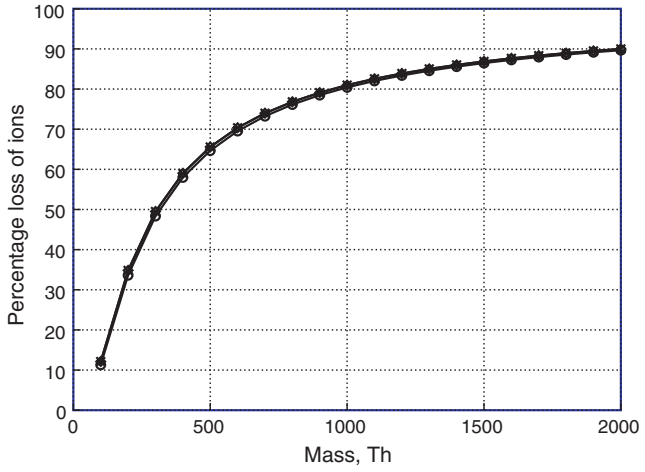

Fig. 10. Comparison of percentage loss of ions versus mass for CIT0 with different endcap hole dimensions: 0% (○), 10% aperture (×) and 30% aperture (◊).

Table 8
Numerically computed $E_{r,peak}(R_{esc})$, A_2 for CIT0 with different aperture dimensions.

Aperture size	Potential applied on ring electrode in V	$E_{r,peak}(R_{esc})$ in V/m	Multipole coefficient A_2
0%	31.4	2976.8142	−0.7397
10%	31.426	2977.9277	−0.7387
30%	32.375	3026.3502	−0.7174

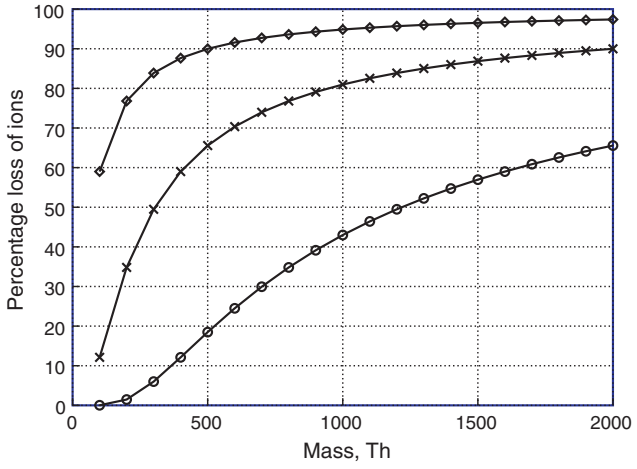

Fig. 11. Comparison of percentage loss of ions versus mass for CIT0 for different RF drive frequencies: 2 MHz (○), 1 MHz (×) and 500 kHz (◊).

It is seen from the figure that the ion loss curves corresponding to these three different cases are overlapping. 0% and the 10% aperture dimension curves shows that the ion loss at a mass of 100 Th is about 12% and it then increases to about 90% at 2000 Th. The ion loss curve corresponding to the 30% aperture dimension reveals that the ion of mass 100 Th is trapped with a loss of about 11% and then increases to about 90% at 2000 Th.

The overlapping nature of these curves can be understood from the closeness of $E_{r,peak}(R_{esc})$ values as seen in Table 8. These trends indicate that aperture size does not play a significant role in ion loss, perhaps, because the radial fields are relatively unaffected by the variation in aperture sizes in the endcap electrodes.

5.3.5. RF drive frequency

The ion loss curves obtained for CIT0 driven at RF drive frequencies of 2 MHz, 1 MHz and 500 kHz are shown in Fig. 11. In these computations, the aperture dimension is set to 10% of the trap radius and the ion temperature is set to 298.15 K. To set a LMCO of 10 Th, the potentials applied to the ring electrodes (with endcaps grounded) are 125.704 V, 31.426 V and 7.856 V for the drive frequencies 2 MHz, 1 MHz and 500 kHz, respectively. All these voltages are set for a computed A_2 of −0.7387. The computed $E_{r,peak}(R_{esc})$ for these sets of parameters are 11911.7110 V/m (for a drive frequency of 2 MHz), 2977.9277 V/m (for a drive frequency of 1 MHz) and 744.4345 V/m (for a drive frequency of 500 kHz). These values are tabulated in Table 9.

Table 9
Numerically computed $E_{r,peak}(R_{esc})$ for CIT0 for different RF drive frequencies.

RF drive frequency	Potential applied on ring electrode in V	$E_{r,peak}(R_{esc})$ in V/m
2 MHz	125.704	11911.7110
1 MHz	31.426	2977.9277
500 kHz	7.856	744.4345

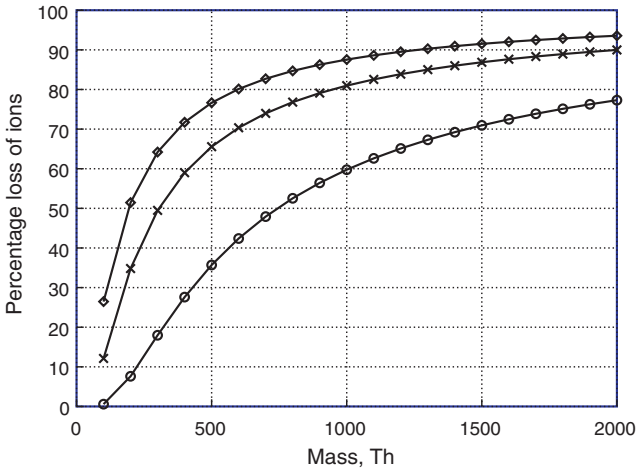

Fig. 12. Comparison of percentage loss of ions versus mass for QIT (○), CIT0 (×) and CITopt (◊).

The lower most curve in the figure, which corresponds to the ion loss in the 2 MHz case, displays a lower ion loss compared to the cases when 1 MHz and 500 kHz are used as drive frequencies in the simulations. The 2 MHz curve shows that a near lossless trapping occurs till a mass of 200 Th and then it increases to about 66% at 2000 Th. In the 1 MHz curve, ion of mass 100 Th is trapped with about 12% loss, after which the ion loss increases to about 90% at 2000 Th. The 500 kHz curve shows no lossless trapping in this mass range, with ion loss rapidly increasing to about 97% for a mass of 2000 Th.

5.4. Comparison of percentage loss of ions for QIT, CIT0 and CITopt

Finally, for the sake of completeness, we demonstrate that the theory developed in this paper can also be used to evaluate the percentage of ion loss in other axially symmetric geometries.

Two additional trap geometries, viz., the QIT and the CITopt are considered and CIT0 has been included in the plots by way of a reference. In these simulations (1) the radius of the ring electrodes of all traps have the same dimension (as shown in Table 1) and (2) the LMCO is set at 10 Th. The imposition of three traps having the same LMCO will cause the applied potential on the ring electrodes to be different for each of the traps. This, of course, causes the trapping conditions in these traps to be different and this may influence the conclusions that are drawn from the results we obtain.

Shown in Fig. 12 are the ion loss curves obtained for the three traps. In these computations, the RF drive frequency is kept at 1 MHz, the aperture dimension is set to 10% of the trap radius and the ion temperature is set at 298.15 K. To set a LMCO of 10 Th, the potentials applied to the ring electrodes (with endcaps grounded) are 23.248 V, 31.426 V and 97.463 V for QIT, CIT0 and CITopt, respectively. $E_{r,\mathrm{peak}}(R_{\mathrm{esc}})$ for these sets of parameters are computed to be 4651.7000 V/m (for the QIT), 2977.9277 V/m (for the CIT0) and 2363.0878 V/m (for the CITopt). These values are tabulated in Table 10. Numerically computed A_2 values are −1.011, −0.7387 and −0.2385, respectively, for the QIT, CIT0 and CITopt.

Table 10
Numerically computed $E_{r,\mathrm{peak}}(R_{\mathrm{esc}})$, A_2 for QIT, CIT0 and CITopt.

Geometry	Potential applied on ring electrode in V	$E_{r,\mathrm{peak}}(R_{\mathrm{esc}})$ in V/m	Multipole coefficient A_2
QIT	23.248	4651.7000	−1.011
CIT0	31.426	2977.9277	−0.7387
CITopt	97.463	2363.0878	−0.2385

From the figure, it is seen that all the curves share a similar trend exhibiting higher loss at a higher masses. It is evident that the QIT has a lower ion loss compared to the two other trap geometries. The ion loss curve corresponding to the QIT reveals that the trapping is almost lossless at a mass of 100 Th and increases slowly to about 77% loss at 2000 Th. The CIT0 ion loss curve shows no lossless trapping, mass 100 Th has about 12% loss with the loss increasing to about 90% at 2000 Th. The ion loss curve corresponding to CITopt indicates that ions are not trapped without loss in the mass range investigated, and increases to about 93% loss at 2000 Th.

6. Concluding remarks

This paper investigates a mechanism of ion loss in ion traps caused by the initial thermal energy associated with the ions. An analytical expression has been developed to estimate the percentage of ions lost as a function of its mass, temperature and escape velocity. We have assumed the velocity distribution of an ensemble of ions of a specific mass to be of the form of a Maxwell velocity distribution. An analytical expression for the escape velocity of an ion has been obtained from the averaged equation of motion. Escape velocity is seen to be a function of the maximum trapping field, mass and frequency of the RF drive. Since the trapping field is determined by both the trap geometry as well as the operating conditions of the trap, it has been possible to evaluate how trap geometries and parameters influence ion loss. This study is concerned with only those ions that have high initial thermal energies located at the trap centre. It ignores other energetic ions which may be present throughout the volume of the trap.

From the simulations carried out it is seen that ion loss, for all the parameters studied, increases with increase in mass. To reduce ion loss and increase sensitivity of the mass analyzer, it is necessary to have lower ion temperatures, operate with higher LMCO, possess a larger trap size, and operate at higher RF drive frequency. The dimension of the aperture in the endcap electrodes do not influence ion loss in the aperture range considered.

We point out that while the analytical expressions presented in this paper are for axially symmetric trap geometries, the theory we have used can be applied for the traps with two-dimensional geometries [3,4] as well. There are, however, several features of these traps that will need to be studied before this theory can be applied. First, in such traps, full three-dimensional simulations have to be carried out, the two-dimensional approximation being inadequate on account of the presence of weak axial fields which prevent escape of ions in the axial direction. Secondly, in these traps the preferred direction of ejection will need to be investigated. While on the one hand there is an equal probability of ejection in the x–y direction, it may turn out that ion escape due to its high thermal energy may occur preferentially in the axial direction because of weaker fields in that direction. This latter study will guide us in creating a surface that should be considered in the Maxwell velocity distribution function. And finally, if the ejection indeed occurs in the axial direction in a few of the traps, there may be a somewhat modified expression for escape velocity.

Although the simulations in this study focused only on ions at the centre of the trap and ignored other high energy ions throughout the volume of the trap, as noted in Section 1, the results presented in this paper are important for the following reason: if in a particular candidate trap there is a high loss of ions from amongst those ions at the centre of the trap, then that particular structure will, in most probability, not be a viable option for consideration. In this sense, this paper provides an insight into the intrinsic limitation of the candidate trap, and would be useful to trap designers investigating novel trap geometries.

Acknowledgements

We thank A.G. Menon and Anindya Chatterjee for discussions during the preparation of this manuscript. We also thank Ms. Sunanda Vinaychandran for copy editing the manuscript. We acknowledge the suggestions provided by two anonymous reviewers of the original manuscript.

References

[1] R.E. March, R.J. Hughes, Quadrupole Storage Mass Spectrometry, Wiley-Interscience, New York, 1989.
[2] G. Wu, R.G. Cooks, Z. Ouyang, Geometry optimization for the cylindrical ion trap: field calculations, simulations and experiments, International Journal of Mass Spectrometry 241 (2005) 119–132.
[3] M.E. Bier, J.E.P. Syka, U.S. Patent 5,420,425 (1995).
[4] Z. Ouyang, G. Wu, Y. Song, H. Li, W.R. Plass, R.G. Cooks, Rectilinear ion trap: concepts, calculations, and analytical performance of a new mass analyzer, Analytical Chemistry 76 (2004) 4595–4605.
[5] P.H. Dawson, Quadrupole Mass Spectrometry and its Applications, Elsevier, Amsterdam, 1976.
[6] E. Fischer, Die dreidimensionale stabilisierung von ladungstragern in einem vierpolfeld, Zeitschrift für Physik 156 (1959) 1–26.
[7] P.H. Dawson, J.W. Hedman, N.R. Whetten, A simple mass spectrometer, Review of Scientific Instruments 40 (1969) 1444.
[8] J. Franzen, R.H. Gabling, M. Shubet, Y. Wang, Practical Aspects of Ion Trap Mass Spectrometry, vol. 1, CRC Press, New York, 1995, Ch. Nonlinear ion traps, p. 69.
[9] J.F.J. Todd, Quadrupole Storage Mass Spectrometry, Wiley-Interscience, New York, 1989, Ch. Historical Review of the Development of the Quadrupole Ion Trap, pp. 16–22.
[10] R.E. March, Quadrupole Ion Traps, Mass Spectrometry Reviews, Wiley Periodicals, Inc. vol. 28, 2009, pp. 961–989.
[11] R.F. Wuerker, H. Shelton, R.V. Langmuir, Electrodynamic containment of charged particles, Journal of Applied Physics 30 (3) (1958) 342–349.
[12] J. Louris, J. Schwartz, G. Stanfford, J. Syka, D. Taylor, Proceedings of the 40th ASMS conference on Mass Spectrometry and Allied Topics, Washington, DC, 1992, p. 1003.
[13] M.G. Blain, L.S. Riter, D. Cruz, D.E. Austin, G. Wu, W.R. Plass, R.G. Cooks, Towards the hand-held mass spectrometer: design considerations, simulation, and fabrication of micrometer-scaled cylindrical ion traps, International Journal of Mass Spectrometry 236 (1–3) (2004) 91–104.
[14] D.E. Austin, D. Cruz, M.G. Blain, Simulations of ion trapping in a micrometer-sized cylindrical ion trap, Journal of the American Society for Mass Spectrometry 17 (3) (2006) 430–441.
[15] F.W. Sears, M.W. Zemansky, University Physics: Mechanics, Heat and Sound, Addison-Wesley Publishing Company, London, 1963.
[16] L.N. Virgin, L.A. Cartee, A note on the escape from a potential well, International Journal of Non-linear Mechanics 26 (1991) 449–452.
[17] G.T. Abraham, A. Chatterjee, A.G. Menon, Escape velocity and resonant ion dynamics in Paul trap mass spectrometers, International Journal of Mass Spectrometry 231 (2004) 1–16.
[18] A. Krishnaveni, N.K. Verma, A.G. Menon, A.K. Mohanty, Numerical observation of preferred directionality in ion ejection from stretched rectilinear ion traps, International Journal of Mass Spectrometry 275 (2008) 11–20.
[19] F.G. Major, H.G. Dehmelt, Exchange-collision technique for the rf spectroscopy of stored ions, Physical Review 170 (1) (1968) 91–107.
[20] R. Blatt, P. Zoller, G. Holzmüller, I. Siemers, Brownian motion of a parametric oscillator: a model for ion confinement in radio frequency traps, Zeitschrift für Physik D Atoms, Molecules and Clusters 4 (1986) 121–126.
[21] K.G. Asano, D.E. Goeringer, S.A. McLuckey, Thermal dissociation in the quadrupole ion trap: ions derived from leucine enkephalin, International Journal of Mass Spectrometry 185–187 (1999) 207–219.
[22] J.N. Louris, J.W. Amy, T.Y. Ridley, R.G. Cooks, Injection of ion into a quadrupole ion trap mass spectrometer, International Journal of Mass Spectrometry and Ion Processes 88 (1989) 97–111.
[23] K.B. Davis, M.-O. Mewes, M.A. Joffe, M.R. Andrews, W. Ketterle, Evaporative cooling of sodium atoms, Physical Review Letters 74 (26) (1995) 5202–5205.
[24] O.J. Luiten, M.W. Reynolds, J.T.M. Walraven, Kinetic theory of the evaporative cooling of a trapped gas, Physical Review A 53 (1) (1996) 381–389.
[25] J. Mikosch, U. Früling, S. Trippel, D. Schwalm, M. Weidemüller, R. Wester, Evaporation of buffer-gas-thermalized anions out of a multipole rf ion trap, Physical Review Letters 98 (22) (2007), 223001–1–223001–4.
[26] J. Mikosch, U. Frühling, S. Trippel, R. Otto, P. Hlavenka, D. Schwalm, M. Weidemüller, R. Wester, Evaporation of trapped anions studied with a 22-pole ion trap in tandem time-of-flight configuration, Physical Review A 78 (2) (2008), 023402–1–023402–13.
[27] P.K. Tallapragada, A.K. Mohanty, A. Chatterjee, A.G. Menon, Geometry optimization of axially symmetric ion traps, International Journal of Mass Spectrometry 264 (2007) 38–52.
[28] E.C. Beaty, Calculated electrostatic properties of ion traps, Physical Review A 33 (6) (1986) 3645–3656.
[29] W.R. Plass, Theory of dipolar dc excitation and dc tomography in the rf quadrupole ion trap, International Journal of Mass Spectrometry 202 (2000) 175–197.
[30] E.R. Badman, R.C. Johnson, W.R. Plass, R.G. Cooks, A miniature cylindrical quadrupole ion trap: simulation and experiment, Analytical Chemistry 70 (1998) 4896–4901.
[31] N.W. McLachlan, Theory and Applications of Mathieu Functions, Clarendon, Oxford, 1947.
[32] E.K. Ganapathy Subramanyan, Escape of high mass ions due to initial thermal energy and its implications for rf trap design, M.Sc. (Engg.) Thesis (under review), Department of Instrumentation, Indian Institute of Science, Bangalore, India.
[33] E. Kreyszig, Advanced Engineering Mathematics, John Wiley & Sons, New York, 2005.